Biosensors and Bioelectronics 143 (2019) 111605

Contents lists available at ScienceDirect

Biosensors and Bioelectronics

journal homepage: www.elsevier.com/locate/bios

A ratiometric multicolor fluorescence biosensor for visual detection of alkaline phosphatase activity via a smartphone

Li Hou[a], Yuxin Qin[a], Jinying Li[a], Siyuan Qin[a], Yuanlin Huang[a], Tianran Lin[a,*], Liangqia Guo[b], Fanggui Ye[a], Shulin Zhao[a]

[a] State Key Laboratory for the Chemistry and Molecular Engineering of Medicinal Resources, College of Chemistry and Pharmaceutical Science, Guangxi Normal University, Guilin, 541004, PR China

[b] Ministry of Education Key Laboratory of Analytical Science of Food Safety and Biology, Fujian Provincial Key Laboratory of Analysis and Detection Technology for Food Safety, College of Chemistry, Fuzhou University, Fuzhou, 350116, PR China

ARTICLE INFO

Keywords:
Multicolor fluorescent biosensor
Smartphone
Alkaline phosphatase
Visual detection
Metal organic framework

ABSTRACT

Herein we designed a selective and smartphone-based strategy for visual detection of alkaline phosphatase (ALP) by utilizing the property of amino-functionalized copper (II)-based metal-organic frameworks (NH_2-Cu-MOFs) with oxidase mimic property and fluorescence property. Surprisingly, the oxidase mimic property of NH_2-Cu-MOFs can work well at a high pH value 8.0. Thus, a cascade reaction between ALP and NH_2-Cu-MOFs was realized for the construction of a ratiometric multicolor sensing platform through the controllable catalytic activity of NH_2-Cu-MOFs by pyrophosphate (PPi) and ALP. The catalytic activity of NH_2-Cu-MOFs was greatly inhibited because of the binding ability of Cu^{2+} with PPi. When the ALP was added, the catalytic activity of NH_2-Cu-MOFs was restored and then further catalyzed the o-phenylenediamine to form the 2, 3-diaminophenazine due to the hydrolysis function of ALP towards PPi into orthophosphates. RGB analysis of the fluorescent sample images was adopted for ALP quantitative analysis. Besides, a hydrogel test kit and mobile app for ALP detection were designed as conceptual products for point-of-care. The LODs of the fluorescence sensing platform was 0.078 mU mL^{-1} and 0.35 mU mL^{-1} by solution analysis and hydrogel test kit analysis, respectively. This fluorescent visual method was applied to ALP detection in serum samples with satisfying results, which opened a promising horizon for the diagnosis of other biomarkers in clinical serum samples based on ALP-mediated enzyme-linked immunosorbent assay for the development of biomedicine and clinical diagnosis.

1. Introduction

Alkaline phosphatase (ALP), an essential hydrolase enzyme for removing phosphate functional groups from a variety of biomolecules including nucleic acids, proteins, and alkaloids (Dong et al., 2015; Zhang et al., 2017), acts as an important biomarker in the clinical diagnosis of various diseases such as diabetes, bone disease, prostatic cancer, and liver dysfunction. The normal level of ALP in human serum is 40–190 U L^{-1} for adults, and the permittable level in children and pregnant women serum is higher than 500 U L^{-1}(Dong et al., 2015; Hayat and Andreescu, 2013; Qian et al., 2015). The level of ALP in human serum is higher or lower than the normal threshold of ALP which may cause serious illness for human. High ALP contents in serum often relates to osteoblastic bone tumors, osteomalacia, biliary obstruction, leukemoid reaction or lymphoma (Tang et al., 2019). Low ALP contents may arise from some metabolic disorders such as Wilson's diseases or hematological diseases such as aplastic anemia and chronic myelogenous leukemia (Tang et al., 2019). Besides, ALP is widely used in enzyme-linked immunosorbent assay because of its high catalytic activity, broad substrate specificity, easy binding with antibody and mild reaction conditions as well as good stability (Chen et al., 2018; Zhao et al., 2019). Therefore, the establishment of a reliable simple, sensitive, and selective approaches for the detection of ALP level or activity is of significant important for medical diagnoses and biomedical research (Liu et al., 2018).

Considering that the importance of ALP in clinical diagnosis, various methods have been developed for ALP detection, such as colorimetry (Gao et al., 2018), electrochemistry (Mintz Hemed et al., 2018), chemiluminescence (Díaz et al., 2002; Hai et al., 2017), surface-enhanced Raman scattering (Zeng et al., 2017), and fluorescence (Chen et al., 2018). Among various methods, the fluorescence method has attracted increasing research attention owing to its advantages of simplicity and

* Corresponding author.
E-mail address: tianranlin@163.com (T. Lin).

https://doi.org/10.1016/j.bios.2019.111605
Received 9 June 2019; Received in revised form 13 August 2019; Accepted 15 August 2019
Available online 17 August 2019

high sensitivity. For example, Li and his co-workers designed a sensitive fluorescence sensor for ALP analysis based on poly(30T)-templated CuNPs (Li et al., 2017). Pyrophosphate (PPi) can quench the fluorescence of poly(30T)-templated CuNPs and the fluorescence can be restored by the ALP hydrolysis function. Nevertheless, the existing ALP fluorescent assays almost depend on ALP-mediated changes in monochromatic fluorescence of fluorescent nanomaterials (Chen et al., 2018; Li et al., 2017; Sun et al., 2017, 2016; Tang et al., 2019). The fluorescence intensity at a single emission wavelength is susceptible to various environmental factors, including exciting light intensity, emitting light collection efficiency, and fluorescence probe concentration. In addition, the existing single-emission wavelength fluorescence immunoassay method has low color change resolution, which is not conducive to on-site detection and diagnosis. Ratio fluorescence sensing technology with dual-wavelength emission is expected to solve this problem (Deng et al., 2015; Zheng et al., 2014). Ratio-based fluorescence sensing technology provides built-in self-calibration for various analytical-independent factors, with particular attention in analytical sensing and optical imaging, with the capacity to provide the accurate quantitative analysis (Fan et al., 2013; Wu et al., 2016). Zhao et al. developed a ratiometric fluorescence assay for the detection of ALP activity based on the covalent immobilization of fluorescein molecules and electrical adsorption of bisquaternary ammonium salt of TPE (TPE-$2N^+$) onto polyethylene terephthalate (PET) fiber surface (Zhao et al., 2017). Although ratiometric fluorescence sensor is sensitive and accurate, expensive instruments and professional operators should be required which greatly limit its applications for in-field testing, especially for remote areas or resource-constrained regions that do not have enough laboratory resources. Thus, an enormous challenge is still encountered for ratiometric fluorescence sensor which is urgent to discover new ALP sensing strategies with less chemical regents or synthesis requirements, and explore a point-of-care (POC) platform for performing at the point of need, outside the laboratory in daily clinical diagnosis.

In recent years, the smartphone-based detection method for healthcare, food safety, and environmental monitoring has attracted particular attention because smartphone camera has some advantages such as high-resolution imaging, manual or auto exposure and focus control, ease of use, portability, image storage, and programmability (Mahato and Chandra, 2019; Pongnumkul et al., 2015). As a result, this smartphone-based detection method is a good candidate for POC platforms for remote areas or resource-constrained regions where are lack of laboratory resources and expensive instruments. Owing to the characters of LED (light emitting diode) flashlight of the camera, the color image taken by the camera is separated into three colors including red, green, and blue. Typically, the red-green-blue (RGB) values are obtained by analyzing the digital photos with software named ColorSchemer studio or a soft named RGB color picker in a smartphone, which could be as a response signal for quantifying the concentration of various analytes (Lin et al., 2016). Xie et al. developed a colorimetric platform based on urease and ALP catalyzed multicolor generation and simple signal readout with a smartphone via the RGB values (Xie et al., 2018). This method needs no expensive instruments, which opening broad future perspectives for next-generation POC testing. However, bio-enzyme like urease is easy to denature and the sensitivity needs to be improved for early clinical diagnosis. Mahato and his co-workers designed an office punching machine crafted paper biosensor for naked eye detection of ALP in milk samples. The quantitative detection of ALP is done by the RGB values from the smartphone. Although this paper-based detection systems possess the advantage of low price, adequate availability, and environment-friendly nature, the sensitivity of this sensing system for ALP detection is not satisfactory (LOD: 0.87 U mL^{-1}) and the color resolution for visual detection of ALP activity by naked eyes and smartphone is insufficient (Mahato and Chandra, 2019). Both the development of new apps and the continuous improvement of smartphone electronics have paved the way for the use of smartphones as biosensors. Almost all the optical-based methods have been integrated with smartphone, including absorbance, reflectance, fluorescence, surface plasmon resonance (SPR), bio-chemiluminescence and electrochemiluminescence. Accordingly, it is important to explore a simple but effective POC strategy for visual detection of ALP activity by naked eyes and smartphone with high color resolution and high sensitivity.

Recently, metal-organic frameworks (MOFs)-based fluorescence sensing has attracted great attention because both metal ion and organic linkers can be utilized in the generation of luminescence signals. Many works have been focused on the detection of various chemical substances by using fluorescent MOFs-based sensors, including metal ions, explosives, and small molecules (Hu et al., 2018; Lustig et al., 2017). Furthermore, MOFs possesses the enzyme-mimicking catalytic activity which is much more stable in harsh condition such as extreme pH, high salt, high temperature and for long-term storage than natural enzyme (Li et al., 2018). However, most MOFs nanozymes can only work well under an acid environment and using a multifunctional MOFs for the construction of biosensor is still on the early stage (Li et al., 2019; Lin et al., 2018). Inspired by these properties, we want to synthesize a multifunctional MOFs as the nanozyme and fluorescence donor for visual fluorescence detection of ALP under the same pH. Hydrogel is particularly well-suited for the design of visual detection platform owing to its negligible fluorescence emission and background color, as well as its controllable shape and large loading capacity (Lin et al., 2014). Hydrogel kit shows the advantages of simplified operation, portable property and furthermore, less skilled operators are needed in the analysis by using hydrogel kits which is beneficial to end-users.

In this work, a fluorescence sensing platform and hydrogel kit for selective and POC diagnosis of important biomarker ALP in serum was established based on the multifunctional NH_2-Cu-MOFs with oxidase mimetic activity, fluorescent emission, and enzyme cascade activity by combining with the merits of a smartphone (Scheme 1). The coordination-induced assembly of Cu^{2+} and 2-amino-1,4-benzenedicarboxylic acid (ABDC) produced the NH_2-Cu-MOFs with high oxidase mimic property. Interestingly, the oxidase-mimetic activity of NH_2-Cu-MOFs can work well under a high pH value of 8.0. With the addition of PPi, the oxidase-mimetic activity of NH_2-Cu-MOFs was completely suppressed because of the good affinity between Cu^{2+} with PPi. Whereas, when ALP was introduced, PPi was hydrolyzed to orthophosphates (Pi) with low affinity to Cu^{2+}. Therefore, the oxidase-mimetic activity of NH_2-Cu-MOFs was reactivated, and a ratiometric fluorescence sensor was developed for ALP using o-phenylenediamine (OPD) as substrate. The OPD could be oxidized by Cu^{2+} of NH_2-Cu-MOFs and the resultant 2,3-diaminophenazine (oxOPD) solution exhibited a visible pale-yellow color as well as an orange-yellow fluorescence when irradiated by ultraviolet light. The RGB digital color for quantitative analysis of ALP was achieved by a smartphone camera. Additionally, the ratio of the red (R) value to the sum of RGB (R + G + B) values is obtained as response signal which is beneficial to improve the accuracy of the results through self-calibration of two dissimilar wavelengths. In this regard, the quantitative, real-time detection of ALP activity is exhibited using a simple readout platform by a smartphone camera and a hand-held UV lamp, which opened a promising horizon for the diagnosis of other biomarkers in clinical serum samples based on ALP-mediated enzyme-linked immunosorbent assay for the development of biomedicine and clinical diagnosis.

2. Experimental section

The chemicals and apparatuses used in the experiment and the experimental procedures are detailed in the supplementary information (SI).

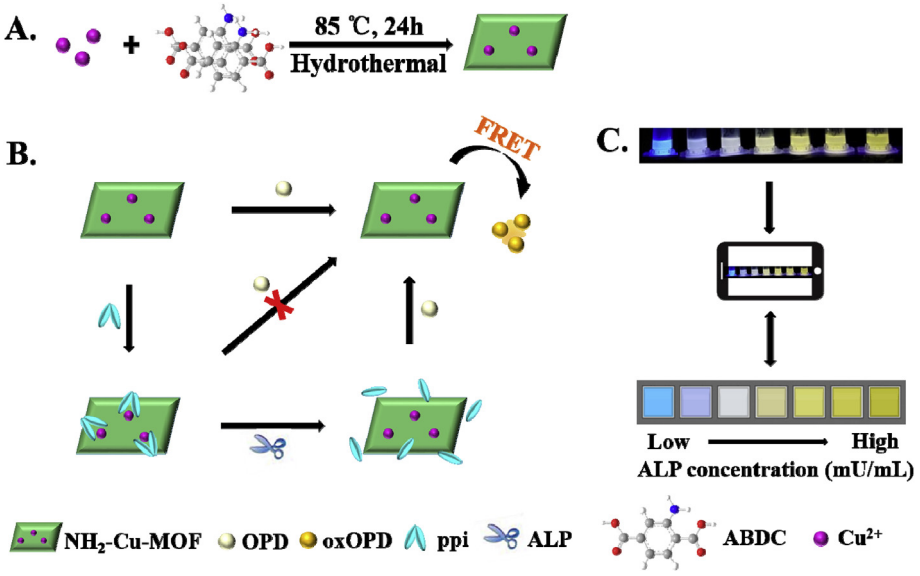

Scheme 1. Schematic illustration of a ratiometric multicolor fluorescence biosensor for visual detection of alkaline phosphatase activity via a smartphone.

3. Results and discussion

3.1. Characterization of NH_2-Cu-MOFs

SEM and TEM were employed for characterization of the morphology of the NH_2-Cu-MOFs. As seen in Fig. 1A and Fig. 1B, the as-prepared NH_2-Cu-MOFs showed cuboid-like shape with a mean length of 200 ± 30 nm and a width of 130 ± 35 nm. EDS mapping (Fig. S1) and XPS analysis (Fig. S2) confirmed the presence of C, Cu, N and O elements on NH_2-Cu-MOFs. As shown in Fig. S2A, the binding energy of Cu $2p_{3/2}$ and Cu $2p_{1/2}$ of Cu in NH_2-Cu-MOFs was 934.3 eV and 953.8 eV, respectively, the result was consistent with that of Cu $(NO_3)_2$ (Shen et al., 2015). The binding energy of 939.5 eV and 962.8 eV was attributed to the Open 3d shell of Cu^{2+} (Shen et al., 2015). However, the binding energy of Cu^0 and Cu^+ was undetected, further confirming that copper existed as Cu^{2+}. In Fig. S2B, only one peak at 399.7 eV was observed in the N 1s spectrum, which was probably due to the presence of an amino group (C-N-H) (Lin and Wang, 2013; Zhan and Zeng, 2016). The high-resolution asymmetric C 1s XPS spectra were showed in Fig. S1C, three peaks were located at 288.3, 286.3 and 284.6 eV corresponding to the C=O, C-O, and C-C (sp^2), respectively (Ren et al., 2015). Fig. S1D showed that the high-resolution XPS spectra of O 1s was at 531.3 eV and 533.0 eV corresponding to C=O and C–OH/C–O–OH/N–O–C (Qin et al., 2015). The XRD patterns of NH_2-Cu-MOFs were shown in Fig. 1C. The as-prepared MOFs had a characteristic diffraction peak which was consistent with the standard diffraction data (CCDC-687690) (Carson et al., 2009), demonstrating that the NH_2-Cu-MOFs was well crystallized (Rodenas et al., 2015). The chemical

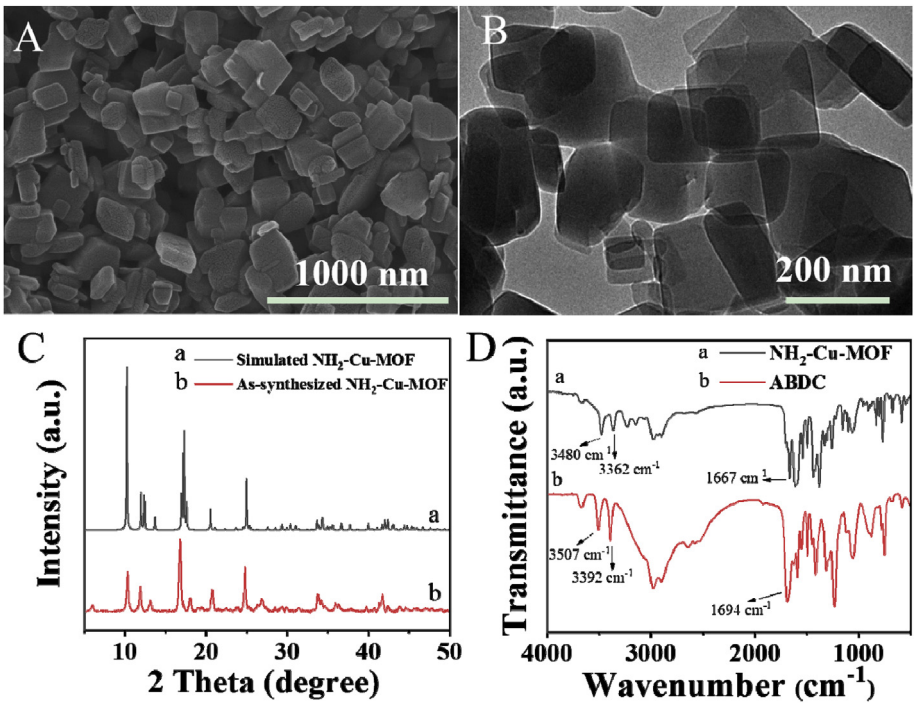

Fig. 1. (A) SEM image and (B) TEM image of NH_2-Cu-MOFs, (C) XRD pattern for NH_2-Cu-MOFs (line b) and the simulated XRD pattern for the NH_2-Cu-MOFs (line a), and (D) FTIR spectrum for NH_2-Cu-MOFs (line a) and bridging ligand (ABDC, line b).

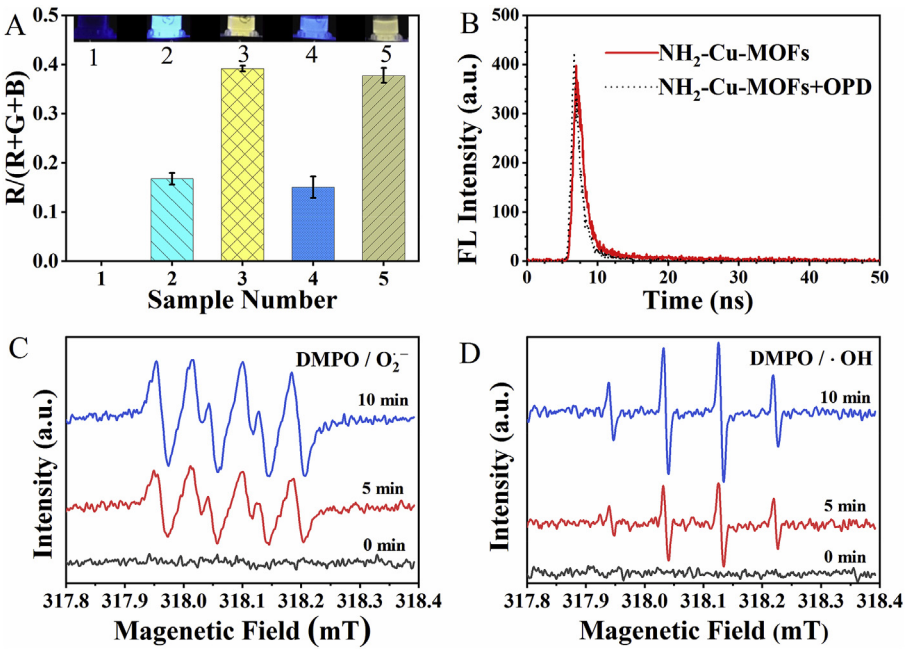

Fig. 2. (A) Photos and RGB signal of (1) OPD, (2) NH_2-Cu-MOFs, (3) NH_2-Cu-MOFs + OPD, (4) NH_2-Cu-MOF + PPi + OPD, (5) NH_2-Cu-MOF + ALP + PPi + OPD in 50 mmol L^{-1} Tris-HCl buffer at pH 7.2. The corresponding photos are under ultraviolet light (365 nm). The final concentrations of the OPD, NH_2-Cu-MOFs, PPi, and ALP are 6.5 mmol L^{-1}, 0.02 mg mL^{-1}, 0.40 mmol L^{-1}, 90 mU mL^{-1}, respectively. (B) Time-resolved fluorescence decay curves of NH_2-Cu-MOFs in the absence (red curve) and presence (black curve) of OPD. ESR spectra for (C) $O_2^{\bullet -}$ and(D)•OH. (For interpretation of the references to color in this figure legend, the reader is referred to the Web version of this article.)

structure of the NH_2-Cu-MOFs and the ligand (ABDC) were analyzed (Fig. 1D), the C=O stretching vibration absorption peak of ligand ABDC was at 1694 cm^{-1} (line a in Fig. 1D). However, it changed to the 1667 cm^{-1} which indicated the Cu^{2+} coordination was formed in the NH_2-Cu-MOFs (line b). Two absorption peaks at 3507 and 3392 cm^{-1} which were attributed to the symmetrical and asymmetric stretching vibrations of $-NH_2$ shifted to 3480 and 3362 cm^{-1}, respectively. These results indicated that NH_2-Cu-MOFs was successfully synthesized.

3.2. Sensing principle

To illustrate the feasibility of the sensing principle for visual detection of ALP, RGB values were detected by a smartphone when the sensing system was under the ultraviolet light with 365 nm. The fluorescent color change of the samples (inset of Fig. 2A) can be transduced into the change in R/(R + G + B) value. As shown in Fig. 2A, The OPD solution (Sample 1) was non-fluorescence and NH_2-Cu-MOFs (Sample 2) exhibited a blue fluorescence under 365 nm UV light. It is interesting that a strong yellow fluorescence was observed after the addition of NH_2-Cu-MOFs into the non-fluorescent OPD solution (Sample 3 in Fig. 2A). The results indicated that NH_2-Cu-MOFs showed oxidase-mimetic activity and the oxidation reaction towards OPD catalyzed by NH_2-Cu-MOFs was triggered and produced oxOPD with yellow fluorescence. Sequently, when the PPi was added into the above-mixed solution (Sample 4 in Fig. 2A), the fluorescent intensity was decreased and the color of the solution was turned to pale blue. Due to the preferential affinity of PPi to Cu^{2+} of NH_2-Cu-MOFs (Sun et al., 2016), the catalytic function of NH_2-Cu-MOFs towards OPD could be partially inhibited, resulting in the decrease of fluorescence color of mixed solution. However, the addition of ALP into the PPi catalyzed the hydrolysis of PPi into Pi and regained the oxidase-mimetic activity of NH_2-Cu-MOFs by disabling the PPi-based complexation. The solution exhibited yellow fluorescence which indicated the oxidation of OPD (Sample 5 in Fig. 2A). Additionally, in the absence of NH_2-Cu-MOFs, the PPi and ALP had negligible interference on the fluorescence of the initial OPD solution (data not shown). More importantly, these processes could be detected via RGB values of corresponding photos by smartphone under ultraviolet light (Fig. 2A). Therefore, these results illustrated that a ratiometric multicolor fluorescence biosensor can be designed for the visual detection of ALP via a smartphone.

To understand the mechanism of the oxidase-mimetic activity of NH_2-Cu-MOFs, the fluorescence lifetime of NH_2-Cu-MOFs before and after reactions was tested. In Fig. 2B, the lifetime of NH_2-Cu-MOFs was 1.30 ns. After the generation of oxOPD, the fluorescence lifetime of NH_2-Cu-MOFs was decreased to 1.01 ns, demonstrating that the fluorescence quenching of NH_2-Cu-MOFs triggered by oxOPD was due to the dynamic quenching effect. Firstly, NH_2-Cu-MOFs as donor molecules were excited by a certain frequency of photons. When the NH_2-Cu-MOFs were in the process of returning to the ground state, the energy was transferred to the adjacent receptor molecule oxOPD, and accompanied by a decrease in fluorescence lifetime via fluorescence resonance energy transfer (FRET). Therefore, a ratiometric fluorescence sensor based on FRET was successfully designed.

Furthermore, the ESR was performed to detect the probable generated free radical during the catalytic reaction (Fig. 2CD). Generally, 5, 5-Dimethyl-1-pyrroline N-oxide (DMPO) was used as a spin trap to capture ROS (•OH and $O_2^{\cdot -}$). As seen in Fig. 2CD, the relative intensities enhanced with the increasing incubation time of DMPO and NH_2-Cu-MOFs. Meanwhile, the ESR spectrum of NH_2-Cu-MOFs exhibited four main peaks with the relative intensities of 1:1:1:1 (Fig. 2C) and 1:2:2:1 (Fig. 2D), which were assigned as the specific signals of DMPO/$O_2^{\cdot -}$ and DMPO/•OH, respectively. These results demonstrated that $O_2^{\cdot -}$ and •OH were generated from the oxidase mimetic activity of NH_2-Cu-MOFs and resulted in the oxidation of OPD.

To verify whether the PPi can bind NH_2-Cu-MOFs, energy-dispersive X-ray spectroscopy (EDS) element analysis was used to analyze the product obtained from the reaction of NH_2-Cu-MOFs with PPi. Before measurement, the PPi was blended with NH_2-Cu-MOFs for a moment and then washed with deionized water by centrifugation. As shown in Fig. S3, Cu, C, N, O, P elements were detected. By comparison with the XPS spectra of Fig. S2, a new element of P could be observed obviously in Fig. S3, which was ascribed to the presence of PPi. Thus, these results demonstrated the complexation affinity of NH_2-Cu-MOFs and PPi.

3.3. Optimization of fluorescence detection parameters

To acquire an optimal analytical performance, the experimental conditions such as pH of assay solution, incubation temperature, the OPD concentration, the incubation time between OPD and NH_2-Cu-MOFs, the incubation time between PPi and NH_2-Cu-MOFs and the concentration of PPi as well as the incubation time of between PPi and ALP have been optimized. Firstly, the catalytic activity of NH_2-Cu-MOFs

at various pH was investigated. As seen in Fig. S4A, the R/(R + G + B) gradually increased with the increase of pH in the range of 4.0–7.2 and tended to decrease with a pH higher than 8.0, indicating the catalytic activity of the NH_2-Cu-MOFs towards OPD oxidation with an optimal pH value at 7.2. Meanwhile, the catalytic activity of NH_2-Cu-MOFs at various temperatures was also monitored. As a result, the optimal temperature for NH_2-Cu-MOFs was 37 °C (Fig. S4B).

Furthermore, the effect of OPD concentration on the oxidase mimetic activity of NH_2-Cu-MOFs was investigated. As seen in Fig. S4C, the catalytic activity of NH_2-Cu-MOFs increased with the increasing OPD concentrations from 0 to 6.4 mmol L^{-1}, and then nearly invariable between the concentration of 6.4 mmol L^{-1} and 9.0 mmol L^{-1} which suggested the optimal OPD concentration was 6.4 mmol L^{-1}. As indicated in Fig. S4D, the ratio values increased with the increasing incubation time between OPD and NH_2-Cu-MOFs, and tended to be a plateau when the incubation time was higher than 60 min. Therefore, 60 min was selected as the optimal incubation time of OPD and NH_2-Cu-MOFs.

The effects of PPi concentration and the incubation time between PPi and NH_2-Cu-MOFs on the oxidase mimetic activity of NH_2-Cu-MOFs were examined next. PPi, which could coordinate with NH_2-Cu-MOFs, would inhibit the oxidase mimetic activity of NH_2-Cu-MOFs toward the catalysis oxidation of OPD. With the concentration of PPi increased, the inhibition effect of PPi toward the NH_2-Cu-MOFs got enlarged. Fig. S4E showed that ratio values decreased rapidly with increasing concentrations of PPi from 0 to 0.40 mmol L^{-1} and decreased slowly at PPi concentration from 0.40 to 1.5 mmol L^{-1}. Typically, the excessively high concentrations of PPi might cause non-productive hydrolysis by ALP, which would have a negative effect on detection sensitivity. Therefore, a PPi concentration of 0.40 mmol L^{-1} was selected in the experiment. In order to investigate whether the incubation time between PPi and NH_2-Cu-MOFs influences the oxidase mimetic activity of the NH_2-Cu-MOFs, the incubation time was optimized. The data in Fig. S4F demonstrated that the PPi inhibition of the catalysis activity of NH_2-Cu-MOFs was not dependent on the incubation time. Nevertheless, consideration of the whole assay time, the final incubation time between PPi and NH_2-Cu-MOFs was established at 10 min. The incubation time between PPi and ALP was optimized (Fig. S4G). The ratio values were increased with the increasing incubation time and then reached a plateau when the incubation time was more than 30 min. Finally, 30 min was selected as the optimal incubation time for MOFs-PPi and ALP. Therefore, the above results further demonstrate that PPi can suppress the oxidase-mimetic activity of NH_2-Cu-MOFs and ALP can indeed relieve the PPi-induced confinement.

3.4. Analytical performance

To evaluate the sensitivity of the developed NH_2-Cu-MOFs-based fluorescent sensor platform, we measured ALP standard solutions with various concentrations under the optimal experimental conditions. As seen in Fig. 3A, with the increasing concentrations of ALP, the degree of oxidation of OPD got higher and resulted in the obvious color change from blue to enhanced yellow fluorescence under irradiation with 365 nm UV light. As seen in Fig. 3B, the △R/(R + G + B) values increased with the increscent logarithm of ALP concentrations in the range from 2 mU mL^{-1} to 180 mU mL^{-1} corresponding to Fig. 3A. The linear regression equation was △R/(R + G + B) = 0.1596 × log ($C_{[ALP]}$/mU mL^{-1}) - 0.1037 (R^2 = 0.9828), and the limit of detection (LOD) was calculated as 0.078 mU mL^{-1} (S/N = 3). Moreover, as a conceptual design, the sensory hydrogels were applied for ALP detection over the range of 5–120 mU mL^{-1}, and a portable hydrogels test kit for ALP detection was designed. The procedure for the detection of ALP by portable hydrogel test kit and the test result were shown in Fig. S5 and Fig. S6, respectively. The fitted linear regression equation could be expressed as △R/(R + G + B) = 0.05613 × log ($C_{[ALP]}$/mU mL^{-1}) - 0.0221 (R^2 = 0.9940), the LOD was 0.35 mU mL^{-1}. These results indicated that NH_2-Cu-MOFs-based fluorescent sensor platform was suitable for the quantification of ALP in human serum samples. More importantly, the color change induced by the bio-enzyme ALP can be distinguished by the naked eye with easy implementation and satisfying sensitivity, so that this method does not require expensive instruments for the detection of ALP in clinical diagnosis. Additionally, to take full advantage of the RGB analysis method for the analysis of biomarker, an app of mobile phone for the quantitative detection of ALP was designed and a definite reference value of biomarker concentration can be obtained by simple click (Fig. S7). These results show a potential application for the biomarker analysis as a point of care strategy.

3.5. Investigation of ALP inhibitors

To investigate the possibility of the proposed methods for evaluating enzyme inhibitor efficiency of ALP, Na_3VO_4, a common ALP inhibitor, was used for the test. As shown in Fig. 4, when Na_3VO_4 was added to the sensing system, the hydrolysis of PPi was restricted because of the inhibition of ALP by Na_3VO_4, which resulted in the depression of the ΔR/(R + G + B). It was found that the activity of ALP was inhibited when the concentration of Na_3VO_4 was increased from 0 to 150 mmol L^{-1}, and the ratio values exhibited a gradual decrease and fluorescence colors of the solution changed from yellow to blue color which suggested that this method could be applied for evaluating the inhibitor efficiency.

3.6. The selectivity of the sensing method

To evaluate the specificity of the NH_2-Cu-MOFs-based fluorescent sensor platform, we studied the effect of several enzymes which coexisted with ALP in the clinical serum, including proteinase K, glucose oxidase, acetylcholinesterase, tyrosinase, cholesterol oxidase, lysozyme, uricase, and PPase under the same experimental conditions. Compared with the signal produced by ALP assay, significant decreases of ΔR/(R + G + B) value induced by the nonspecific proteins were observed in Fig. 5A. Furthermore, the interference experiments for PPi was also investigated including $H_2PO_4^-$, HPO_4^{2-}, PO_4^{3-}, Cl^-, NO_3^-, SO_4^{2-} and HCO_3^-. The results in Fig. 5B indicated the above-coexisted anion

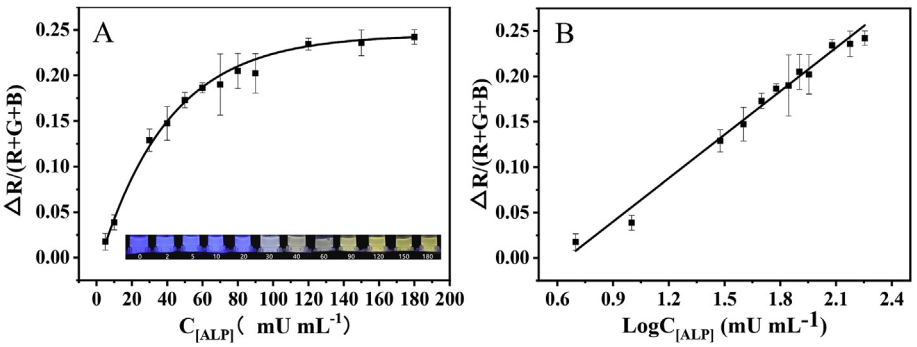

Fig. 3. (A) Quantitative detection of ALP by analyzing the △R/(R + G + B) values of digital photos versus the ALP concentrations. Inset of Fig. 3A show the evolution of corresponding colors under 365 nm UV lamp for various concentrations of ALP (mU mL^{-1}, from left to right: 0, 2, 5, 10, 20, 30, 40, 60, 90, 120, 150, 180); (B) The linear calibration plots (log *C vs.* $^{\triangle}R/(R + G + B)$) for ALP detection (error bars: SD, n = 3). (For interpretation of the references to color in this figure legend, the reader is referred to the Web version of this article.)

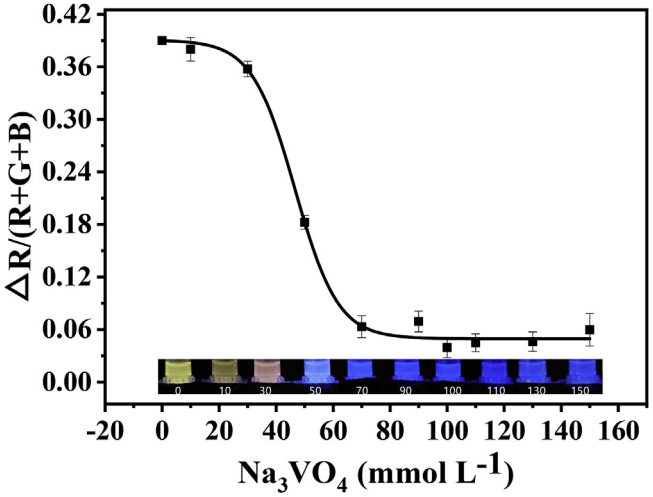

Fig. 4. Kinetic plots of the corresponding △R/(R + G + B) values against the Na_3VO_4 concentration (error bars: SD, n = 3). Inset is the photos of NH_2-Cu-MOFs-PPi-based ALP activity inhibition bioassay system prepared by the addition of different concentrations of Na_3VO_4 (from left to right: 0, 10, 30, 50, 70, 90, 100, 110, 130, 150 mmol L^{-1}) into the mixtures containing NH_2-Cu-MOFs, PPi and OPD in the Tris-HCl buffer.

ions had a negligible effect on the fluorescent intensity of NH_2-Cu-MOFs. These results demonstrated the satisfactory selectivity of the NH_2-Cu-MOFs-based fluorescent sensor platform owing to the strong coordination interaction between PPi and NH_2-Cu-MOFs and the specific catalytic activity of ALP towards PPi.

3.7. Analytical application in real samples and evaluation of method accuracy

To assess potential applicability of the NH_2-Cu-MOFs-based fluorescent sensor platform for real samples, we collected 8 clinical human serum samples with different ALP concentrations from the Guilin Hospital of Chinese Traditional and Western Medicine according to the rules of the local ethical committee. Half of the human serum samples were tested by using the conventional solution test (Table S1), and the other half were tested by using the portable hydrogels test kits (Table S2). Before measurement, two groups of clinical serum samples with 25 times dilution ratios and 8 times dilution ratios were diluted, respectively, because ALP levels in original serum samples were over the linear range. As shown in Table S1 and Table S2, the results obtained from both methods were in good agreement with the referenced values which were obtained from commercialized Roche C501 Automatic Biochemical Analyzer (Switzerland), and the recoveries obtained from both methods were 98.0–103.8% and 98.0–100.5% with RSD in the range of 0.8–3.4% and 1.5–4.8%, respectively, indicating an acceptable accuracy and reproducibility of the proposed NH_2-Cu-MOFs-based fluorescent sensor platform for the application of biomedicine and clinical diagnosis.

4. Conclusions

In summary, we have successfully established a simple, selective and multifunctional NH_2-Cu-MOFs-based fluorescent sensor platform for visual and smartphone-based detection of ALP. The multifunctional NH_2-Cu-MOFs were demonstrated to show the three kinds of functions including oxidase mimetic activity, fluorescent emission property, and enzyme cascade activity. Moreover, ALP concentration can be determined visually by a smartphone without any specialist facilities or healthcare professionals. Preferably, application of the ratiometric measurement in NH_2-Cu-MOFs-based fluorescent sensor platform has the capability of self-calibration by removing the uncertain fluctuations caused by instrumental or complex environmental factors, improving the reproducibility and robustness of MOFs-based fluorescent sensor platform. Therefore, NH_2-Cu-MOFs-based ratiometric fluorescence sensing platform combining with the app and hydrogel kits possesses the advantage of visualization, portability, and ease-of-use, which can be acted as a POC strategy in the field for a large-scale screening of ALP. Certainly, the present work still has its limitations. For example, the stability of the hydrogel kits needs to be studied. And the present work has not been applied to the detection of other biomarkers. Further studies aim to investigate the storage stability of the hydrogel kits by optimizing additional parameters, and explore app applications towards ALP-based fluorescence enzyme-linked immunoassay for the detection of other biomarkers, which is of positive significance for the development of biomedicine and clinical diagnosis.

Conflict of interests

The authors declare that they have no known competing for financial interests or personal relationships that could have appeared to influence the work reported in this paper.

Compliance with ethical standards

All experiments were performed in compliance with the relevant laws and institutional guidelines, and the institutional committee has approved the experiments.

CRediT authorship contribution statement

Li Hou: Conceptualization, Methodology, Funding acquisition, Formal analysis, Writing - original draft, Writing - review & editing. **Yuxin Qin:** Conceptualization, Methodology, Writing - original draft. **Jinying Li:** Methodology. **Siyuan Qin:** Methodology. **Yuanlin Huang:** Methodology, Formal analysis. **Tianran Lin:** Conceptualization,

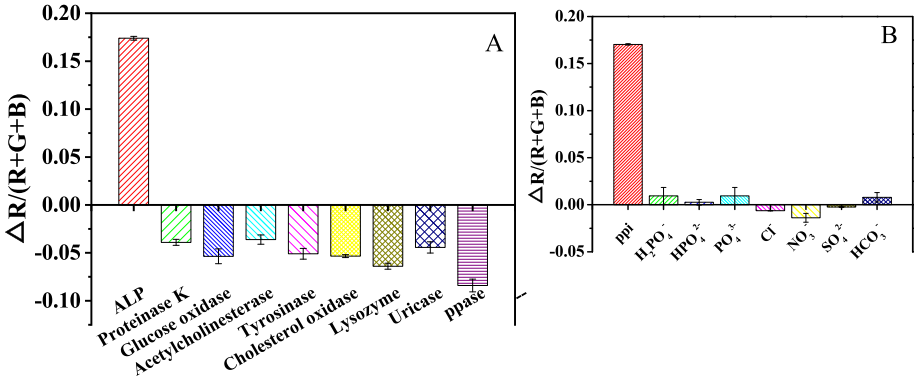

Fig. 5. (A) Specificity of the proposed assay for ALP by RGB analysis. The concentration of ALP, uricase, and PPase was 90 mU mL^{-1} and the concentration of other enzymes was 450 mU mL^{-1}, and (B) anti-interferential tests of the proposed fluorescence platform for PPi. The final concentration of $H_2PO_4^-$, HPO_4^{2-}, PO_4^{3-}, Cl^-, NO_3^-, SO_4^{2-} and HCO_3^- was 2.0 mmol L^{-1} and the final concentration of PPi was 0.40 mmol L^{-1} (error bars: SD, n = 3).

Funding acquisition, Formal analysis, Writing - original draft, Writing - review & editing. **Liangqia Guo:** Formal analysis. **Fanggui Ye:** Formal analysis, Funding acquisition. **Shulin Zhao:** Formal analysis, Funding acquisition.

Acknowledgements

The authors are grateful for financial support from the National Natural Science Foundation of China (21575031, 21365005), the Natural Science Foundation of Guangxi (2018GXNSFBA050053, 2018GXNSFBA281053), Key Project of Guangxi Normal University (2017ZD003, 2017ZD005), Open Project Program of Key Laboratory for Analytical Science of Food Safety and Biology, Ministry of Education and the Program for BAGUI Scholar.

Appendix A. Supplementary data

Supplementary data to this article can be found online at https://doi.org/10.1016/j.bios.2019.111605.

References

Carson, C.G., Hardcastle, K., Schwartz, J., Liu, X., Hoffmann, C., Gerhardt, R.A., Tannenbaum, R., 2009. Synthesis and structure characterization of copper terephthalate metal-organic frameworks. Eur. J. Inorg. Chem. 2009, 2338–2343. https://doi.org/10.1002/ejic.200801224.

Chen, C., Zhao, J., Lu, Y., Sun, J., Yang, X., 2018. Fluorescence immunoassay based on the phosphate-triggered fluorescence turn-on detection of alkaline phosphatase. Anal. Chem. 90, 3505–3511. https://doi.org/10.1021/acs.analchem.7b05325.

Deng, J., Yu, P., Wang, Y., Mao, L., 2015. Real-time ratiometric fluorescent assay for alkaline phosphatase activity with stimulus responsive infinite coordination polymer nanoparticles. Anal. Chem. 87, 3080–3086. https://doi.org/10.1021/ac504773n.

Díaz, A.N., Sánchez, F.G., Ramos, M.C., Torijas, M.C., 2002. Horseradish peroxidase sol-gel immobilized for chemiluminescence measurements of alkaline-phosphatase activity. Sens. Actuators B Chem. 82, 176–179. https://doi.org/10.1016/S0925-4005(01)01003-6.

Dong, L., Miao, Q., Hai, Z., Yuan, Y., Liang, G., 2015. Enzymatic hydrogelation-induced fluorescence turn-off for sensing alkaline phosphatase in vitro and in living cells. Anal. Chem. 87, 6475–6478. https://doi.org/10.1021/acs.analchem.5b01657.

Fan, J., Hu, M., Zhan, P., Peng, X., 2013. Energy transfer cassettes based on organic fluorophores: construction and applications in ratiometric sensing. Chem. Soc. Rev. 42, 29–43. https://doi.org/10.1039/c2cs35273g.

Gao, J., Jia, M., Xu, Y., Zheng, J., Shao, N., Zhao, M., 2018. Prereduction-promoted enhanced growth of silver nanoparticles for ultrasensitive colorimetric detection of alkaline phosphatase and carbohydrate antigen 125. Talanta 189, 129–136. https://doi.org/10.1016/j.talanta.2018.06.064.

Hai, Z., Li, J., Wu, J., Xu, J., Liang, G., 2017. Alkaline phosphatase-triggered simultaneous hydrogelation and chemiluminescence. J. Am. Chem. Soc. 139, 1041–1044. https://doi.org/10.1021/jaci.6bll041.

Hayat, A., Andreescu, S., 2013. Nanoceria particles as catalytic amplifiers for alkaline phosphatase assays. Anal. Chem. 85, 10028–10032. https://doi.org/10.1021/ac4020963.

Hu, S., Yan, J., Huang, X., Guo, L., Lin, Z., Luo, F., Qiu, B., Wong, K.Y., Chen, G., 2018. A sensing platform for hypoxanthine detection based on amino-functionalized metal organic framework nanosheet with peroxidase mimic and fluorescence properties. Sens. Actuators B Chem. 267, 312–319. https://doi.org/10.1016/j.snb.2018.04.055.

Li, J., Si, L., Bao, J., Wang, Z., Dai, Z., 2017. Fluorescence regulation of poly (thymine)-templated copper nanoparticles via an enzyme-triggered reaction toward sensitive and selective detection of alkaline phosphatase. Anal. Chem. 89, 3681–3686. https://doi.org/10.1021/acs.analchem.6b05112.

Li, S., Hu, X., Chen, Q., Zhang, X., Chai, H., Huang, Y., 2019. Introducing bifunctional metal-organic frameworks to the construction of a novel ratiometric fluorescence sensor for screening acid phosphatase activity. Biosens. Bioelectron. 137, 133–139. https://doi.org/10.1016/j.bios.2019.05.010.

Li, S., Liu, X., Chai, H., Huang, Y., 2018. Recent advances in the construction and analytical applications of metal-organic frameworks-based nanozymes. TrAC Trends Anal. Chem. 105, 391–403. https://doi.org/10.1016/j.trac.2018.06.001.

Lin, T., Qin, Y., Huang, Y., Yang, R., Hou, L., Ye, F., Zhao, S., 2018. A label-free fluorescence assay for hydrogen peroxide and glucose based on the bifunctional MIL-53(Fe) nanozyme. Chem. Commun. 54, 1762–1765. https://doi.org/10.1039/c7cc09819g.

Lin, T., Wu, Y., Li, Z., Song, Z., Guo, L., Fu, F., 2016. Visual monitoring of food spoilage based on hydrolysis-induced silver metallization of Au nanorods. Anal. Chem. 88, 11022–11027. https://doi.org/10.1021/acs.analchem.6b02870.

Lin, T., Zhong, L., Guo, L., Fu, F., Chen, G., 2014. Seeing diabetes: visual detection of glucose based on the intrinsic peroxidase-like activity of MoS_2 nanosheets. Nanoscale 6, 11856–11862. https://doi.org/10.1039/c4nr03393k.

Lin, Z., Wang, X., 2013. Nanostructure engineering and doping of conjugated carbon nitride semiconductors for hydrogen photosynthesis. Angew. Chem. Int. Ed. 52, 1735–1738. https://doi.org/10.1002/anie.201209017.

Liu, S.G., Han, L., Li, N., Xiao, N., Ju, Y.J., Li, N.B., Luo, H.Q., 2018. A fluorescence and colorimetric dual-mode assay of alkaline phosphatase activity: via destroying oxidase-like CoOOH nanoflakes. J. Mater. Chem. B 6, 2843–2850. https://doi.org/10.1039/c7tb03275g.

Lustig, W.P., Mukherjee, S., Rudd, N.D., Desai, A.V., Li, J., Ghosh, S.K., 2017. Metal-organic frameworks: functional luminescent and photonic materials for sensing applications. Chem. Soc. Rev. 46, 3242–3285. https://doi.org/10.1039/c6cs00930a.

Mahato, K., Chandra, P., 2019. Paper-based miniaturized immunosensor for naked eye ALP detection based on digital image colorimetry integrated with smartphone. Biosens. Bioelectron. 128, 9–16. https://doi.org/10.1016/j.bios.2018.12.006.

Mintz Hemed, N., Convertino, A., Shacham-Diamand, Y., 2018. Alkaline phosphatase detection using electrochemical impedance of anti-alkaline phosphatase antibody (Ab354) functionalized silicon-nanowire-forest in phosphate buffer solution. Sens. Actuators B Chem. 259, 809–815. https://doi.org/10.1016/j.snb.2017.12.136.

Pongnumkul, S., Chaovalit, P., Surasvadi, N., 2015. Applications of smartphone-based sensors in agriculture: a systematic review of research. J. Sensors 1–18. https://doi.org/10.1155/2015/195308.

Qian, Z., Chai, L., Tang, C., Huang, Y., Chen, J., Feng, H., 2015. Carbon quantum dots-based recyclable real-time fluorescence assay for alkaline phosphatase with adenosine triphosphate as substrate. Anal. Chem. 87, 2966–2973. https://doi.org/10.1021/ac504519b.

Qin, J., Wang, S., Ren, H., Hou, Y., Wang, X., 2015. Photocatalytic reduction of CO_2 by graphitic carbon nitride polymers derived from urea and barbituric acid. Appl. Catal. B Environ. 179, 1–8. https://doi.org/10.1016/j.apcatb.2015.05.005.

Ren, H., Shao, H., Zhang, L., Guo, D., Jin, Q., Yu, R., Wang, L., Li, Y., Wang, Y., Zhao, H., Wang, D., 2015. A new graphdiyne nanosheet/Pt nanoparticle-based counter electrode material with enhanced catalytic activity for dye-sensitized solar cells. Adv. Energy Mater. 5, 1500296. https://doi.org/10.1002/aenm.201500296.

Rodenas, T., Luz, I., Prieto, G., Seoane, B., Miro, H., Corma, A., Kapteijn, F., Llabrés I Xamena, F.X., Gascon, J., 2015. Metal-organic framework nanosheets in polymer composite materials for gas separation. Nat. Mater. 14, 48–55. https://doi.org/10.1038/nmat4113.

Shen, W.J., Zhuo, Y., Chai, Y.Q., Yuan, R., 2015. Cu-based metal-organic frameworks as a catalyst to construct a ratiometric electrochemical aptasensor for sensitive lipopolysaccharide detection. Anal. Chem. 87, 11345–11352. https://doi.org/10.1021/acs.analchem.5b02694.

Sun, J., Mei, H., Gao, F., 2017. Ratiometric detection of copper ions and alkaline phosphatase activity based on semiconducting polymer dots assembled with rhodamine B hydrazide. Biosens. Bioelectron. 91, 70–75. https://doi.org/10.1016/j.bios.2016.12.034.

Sun, J., Wang, B., Zhao, X., Li, Z.J., Yang, X., 2016. Fluorescent and colorimetric dual-readout assay for inorganic pyrophosphatase with Cu^{2+} -triggered oxidation of o-phenylenediamine. Anal. Chem. 88, 1355–1361. https://doi.org/10.1021/acs.analchem.5b03848.

Tang, Z., Chen, H., He, H., Ma, C., 2019. Assays for alkaline phosphatase activity: progress and prospects. TrAC Trends Anal. Chem. 113, 32–43. https://doi.org/10.1016/j.trac.2019.01.019.

Wu, P., Hou, X., Xu, J.J., Chen, H.Y., 2016. Ratiometric fluorescence, electrochemiluminescence, and photoelectrochemical chemo/biosensing based on semiconductor quantum dots. Nanoscale 8, 8427–8442. https://doi.org/10.1039/c6nr01912a.

Xie, W.Y., Lei, L.L., Tian, M.L., Zhang, Z.Y., Liu, Y.S., 2018. A high-resolution colorimetric immunoassay platform realized by coupling enzymatic multicolor generation with smartphone readout. Analyst 143, 2901–2907. http://doi.org/10.1039/c8an00382c.

Zeng, Y., Ren, J.Q., Wang, S.K., Mai, J.M., Qu, B., Zhang, Y., Shen, A.G., Hu, J.M., 2017. Rapid and reliable detection of alkaline phosphatase by a hot spots amplification strategy based on well-controlled assembly on single nanoparticle. ACS Appl. Mater. Interfaces 9, 29547–29553. https://doi.org/10.1021/acsami.7b09336.

Zhan, G., Zeng, H.C., 2016. Synthesis and functionalization of oriented metal-organic-framework nanosheets: toward a series of 2D catalysts. Adv. Funct. Mater. 26, 3268–3281. https://doi.org/10.1002/adfm.201505380.

Zhang, Y., Li, Y., Zhang, C., Zhang, Q., Huang, X., Yang, M., Shahzad, S.A., Lo, K.K.W., Yu, C., Jiang, S., 2017. Fluorescence turn-on detection of alkaline phosphatase activity based on controlled release of PEI-capped Cu nanoclusters from MnO_2 nanosheets. Anal. Bioanal. Chem. 409, 4771–4778. https://doi.org/10.1007/s00216-017-0420-9.

Zhao, J., Wang, S., Lu, S., Liu, G., Sun, J., Yang, X., 2019. Fluorometric and colorimetric dual-readout immunoassay based on an alkaline phosphatase-triggered reaction. Anal. Chem. 91 (12), 7828–7834. https://doi.org/10.1021/acs.analchem.9b01553.

Zhao, L., Xie, S.Z., Song, X.J., Wei, J.J., Zhang, Z., Li, X.H., 2017. Ratiometric fluorescent response of electrospun fibrous strips for real-time sensing of alkaline phosphatase in serum. Biosens. Bioelectron. 91, 217–224. https://doi.org/10.1016/j.bios.2016.12.025.

Zheng, F., Guo, S., Zeng, F., Li, J., Wu, S., 2014. Ratiometric fluorescent probe for alkaline phosphatase based on betaine-modified polyethylenimine via excimer/monomer conversion. Anal. Chem. 86, 9873–9879. https://doi.org/10.1021/ac502500e.